

Synthesis and electrochemical properties of Cr and V-substituted Li_2MnO_3 as cathode materials for secondary lithium batteries

Kyung Wan Kang^a, Yeon Uk Jeong^{a*} and Yong Joong Lee^b

^aSchool of Materials Science and Engineering, Kyungpook National University, Daegu 41566, Korea

^bSchool of Mechanical Engineering, Kyungpook National University, Daegu 41566, Korea

In an attempt to improve the electrochemical performance of Li_2MnO_3 cathode, Cr and V are substituted for Mn via an aqueous reduction reaction followed by heating in air. Li_3VO_4 and Li_2CrO_4 impurities in the as-prepared $\text{Li}_2[\text{Mn}_{1-2x}\text{Cr}_x\text{V}_x]\text{O}_3$ ($0 \leq x \leq 0.2$) samples are removed by washing with deionized (DI) water. Although the washed samples have deficient metal contents, monoclinic layered structures are obtained. $\text{Li}_{1.596}[\text{Mn}_{0.806}\text{Cr}_{0.181}\text{V}_{0.013}]\text{O}_3$ has a composite phase of $\text{Li}_2\text{MnO}_3 \cdot \text{LiCrO}_2 \cdot \text{LiVO}_2 \cdot \text{Li}_4\text{Mn}_5\text{O}_{12}$ and can deliver more than 225mAh/g of discharge capacity above 2.5 V vs. Li at 10 mA/g. Structural changes due to the oxygen loss are minimized, and excellent cycle performance and rate capability have been achieved.

Key words: Secondary lithium batteries, Cathode materials, Li_2MnO_3 , Doping, Structure, Electrochemical properties.

Introduction

Since the secondary lithium batteries have been widely used in consumer electronics as well as in electric vehicles, next generation of secondary lithium batteries demands an enhanced energy density, rate capability, safety, cost, and environmental compatibility. Various types of materials were widely investigated for the use as the cathode of lithium-ion batteries [1]. Among these various cathode materials, LiMO_2 -type structure with a space group of R-3m is stably formed with $M = \text{Co}$ or Ni as the major components in the compounds. Relatively high costs and environmental concern of Co or Ni caused much attention to Mn-based materials. However, among the Li-Mn-O systems, a representative compound of LiMn_2O_4 spinel exhibits relatively small gravimetric and volumetric energy densities in ~ 4 V region and Jahn-Teller effect due to the phase transition in ~ 3 V region. In an attempt to exceed the limited theoretical capacity of LiMO_2 -type cathodes, a new layered structure with higher lithium contents has been investigated [2-4]. Despite the extraction of 2 lithium ions in the layered structure of Li_2MnO_3 give a theoretical capacity of 478 mAh/g, further oxidation of Mn^{4+} is not easy. Moreover, excess lithium ions placed in MnO_6 octahedra layers of $\text{Li}[\text{Li}_{1/3}\text{Mn}_{2/3}]\text{O}_2$ result in low electrical conductivity [5-9].

In order to get $\text{Mn}^{3+/4+}$ couples, it is encouraged to dope pentavalent ion in Li_2MnO_3 . Recently, doping of vanadium ions was pursued but only $\sim 2\%$ could be

substituted and the resulting materials showed improved initial electrochemical performances [10]. Li_2MnO_3 prepared at low temperature and composite of $\text{Li}_2\text{MnO}_3 \cdot \text{LiMO}_2$ ($M = \text{Co}, \text{Ni}, \text{Cr}$) synthesized by the control of lithium and transition metal contents give improved electrochemical behaviors [11-15]. In the case of $\text{Li}[\text{Ni}_x\text{Li}_{1/3-2x/3}\text{Mn}_{2/3-x/3}]\text{O}_2$ which resulted from the solid solution of Li_2MnO_3 and $\text{LiNi}_{1/2}\text{Mn}_{1/2}\text{O}_2$, Ni^{2+} oxidized to Ni^{4+} for the initial stage of charge process. Continued charging gives a flat potential near 4.5 V due to the formation of Li_2O [16]. Due to the structural similarity, Li_2MnO_3 and LiMO_2 ($M = \text{Ni}, \text{Co}, \text{Cr}$) can form nano-composites or solid solutions and achieve a high energy density by offering an additional capacity at high potential regions. Initial charge and discharge capacities are reported to be ~ 300 mAh/g and ~ 250 mAh/g, respectively [12, 17, 18]. In this research, the synthesis of Cr and V-substituted Li_2MnO_3 via aqueous reduction reaction and their electrochemical properties are investigated.

Experimental

$\text{Li}_2[\text{Mn}_{1-x-y}\text{Cr}_x\text{V}_y]\text{O}_3$ ($0 \leq x \leq 0.2$) samples are synthesized by a solution-based reduction reaction. Mixed metal precursors were prepared as follows. 50 ml of 0.25 M V_2O_5 solution was prepared in LiOH aqueous solution and then pH was adjusted to 4 by adding HCl. Various concentrations of 50 ml Cr and Mn solutions were added and mixed in the V solution. 100 ml of 0.5 M solution for reduction was prepared by mixing $\text{LiOH} \cdot \text{H}_2\text{O}$ and KBH_4 in DI water with the ratio of 1 : 2 mol. The mixed metal solution and the reducing solution were simultaneously added to the aqueous NH_4OH solution of pH = 10.5. During the reduction

*Corresponding author:
Tel : +82-53-950-7586
Fax: +82-53-950-5645
E-mail: jeong@knu.ac.kr

reaction, pH was kept at 10.5. The products after the reduction reaction were washed and filtered with DI water followed by drying at 80 °C in air. Pellets were prepared with the mixtures of obtained products and Li_2CO_3 for further heat treatment. Heat treatments were carried out at 900 °C for 12 hours in air. Synthesized products were washed with DI water to remove the impurities followed by heating at 300 °C in air.

X-ray powder diffraction with X'Pert pro MPD (Cu K_α) was carried out to identify the phase and to determine the lattice constants. A field emission scanning electron microscope (FE-SEM, HITACHI S-4200) was used to observe the size and morphology of the powder samples. ICP (Inductively Coupled Plasma, Model Optima7300DV, Perkin Elmer) was used for elemental analysis.

The electrochemical properties were evaluated by using coin cells (2032-type). The slurries were prepared by mixing of 80 wt% of cathode materials, 10 wt% of Super P carbon as a conducting additive, 10 wt% of polyvinylidene fluoride (PVDF) as a binder, and N-methyl pyrrolidone (NMP) as a solvent. Prepared slurries were coated onto an aluminum foil followed by drying in an oven at 120 °C and cold pressing. For electrolytes, 1 M LiPF_6 was dissolved in the mixed solution of ethylene carbonate (EC) and ethyl methyl carbonate (EMC) with the ratio of 1 : 2. Lithium metal was used as the counter electrode and the coin cells were assembled in an Ar-filled glove box. The charge/discharge tests were performed with WBCS3000 (WonATech) between 4.8 and 1.5 V vs. Li with various current densities. 1.0 C-rate was fixed at 150 mA/g. For cyclic voltammetry, the scan rate of 100 $\mu\text{V/s}$ was applied between 4.8 V and 1.5 V vs. Li.

Results and Discussion

Fig. 1 shows the results of X-ray diffraction of the various $\text{Li}_2[\text{Mn}_{1-2x}\text{Cr}_x\text{V}_x]\text{O}_3$ ($0.0 \leq x \leq 0.2$) samples after heating at 900 °C. Impurities of Li_3VO_4 and Li_2CrO_4 are found in Cr and V-doped samples. These impurities can be removed by washing with DI water, and the results of X-ray diffraction are shown in Fig. 2. All samples have monoclinic layered structures with a space group of C2/m. Compared to phase heated at high temperature, low temperature phase does not show clear peaks between $2\theta = 20^\circ$ and 35° , and this is known for the disorder of superlattice [19]. While Li_2MnO_3 heated at 900 °C shows typical XRD patterns of high temperature phase, Cr and V-doped samples also show well developed peaks between $2\theta = 20^\circ$ and 35° [19]. In the case of $x = 0.2$ in $\text{Li}_2[\text{Mn}_{1-2x}\text{Cr}_x\text{V}_x]\text{O}_3$, secondary phase of $\text{Li}_{1+x}\text{Mn}_{2-x}\text{O}_4$ spinel is found. The relatively low ratio of Li/Mn in $\text{Li}_2[\text{Mn}_{1-2x}\text{Cr}_x\text{V}_x]\text{O}_3$ due to the formation of Li_3VO_4 and Li_2CrO_4 impurities is believed to be the reason for $\text{Li}_{1+x}\text{Mn}_{2-x}\text{O}_4$ formation. Table 1 summarizes the results of elemental analysis of

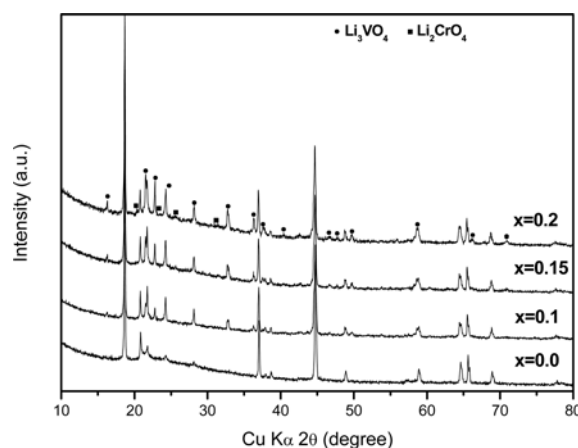


Fig. 1. XRD patterns of the various $\text{Li}_2[\text{Mn}_{1-2x}\text{Cr}_x\text{V}_x]\text{O}_3$ ($0 \leq x \leq 0.2$).

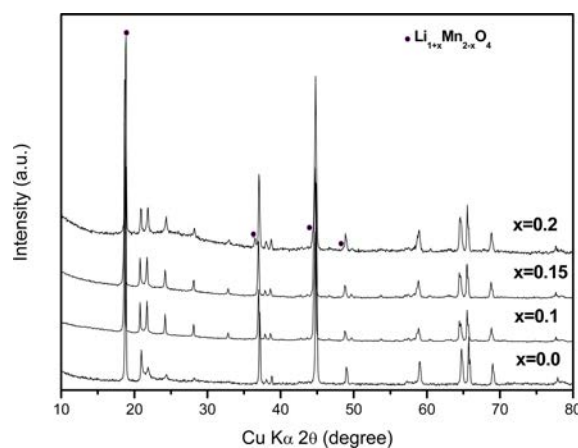


Fig. 2. XRD patterns of various $\text{Li}_2[\text{Mn}_{1-2x}\text{Cr}_x\text{V}_x]\text{O}_3$ ($0 \leq x \leq 0.2$) after washing.

Table 1. The results of elemental analysis of various $\text{Li}_2[\text{Mn}_{1-2x}\text{Cr}_x\text{V}_x]\text{O}_3$ ($0 \leq x \leq 0.2$) after washing.

Target stoichiometry	Elemental analysis			
	Li	Mn	Cr	V
Li_2MnO_3	1.941	1.000	0.000	0.000
$\text{Li}_2[\text{Mn}_{0.8}\text{Cr}_{0.1}\text{V}_{0.1}]\text{O}_3$	1.840	0.918	0.077	0.005
$\text{Li}_2[\text{Mn}_{0.7}\text{Cr}_{0.15}\text{V}_{0.15}]\text{O}_3$	1.781	0.873	0.117	0.010
$\text{Li}_2[\text{Mn}_{0.6}\text{Cr}_{0.2}\text{V}_{0.2}]\text{O}_3$	1.596	0.806	0.181	0.013

various $\text{Li}_2[\text{Mn}_{1-2x}\text{Cr}_x\text{V}_x]\text{O}_3$ ($0 \leq x \leq 0.2$) samples after washing with DI water. The contents of Li, Cr, and V are measured to be lower than the target stoichiometry and this is due to the removal of Li_3VO_4 and Li_2CrO_4 impurities after washing. As Cr and V contents increase, Li/metals ratio decreases in the compounds while the monoclinic layered structures are maintained. Fig. 3 shows S.E.M. images of $\text{Li}_2[\text{Mn}_{1-2x}\text{Cr}_x\text{V}_x]\text{O}_3$ ($0 \leq x \leq 0.2$) after washing. The average particle size of the samples are decreased with the increase in x . The higher doping amount leads to the higher uniformity of the particle size.

The first charge/discharge profiles of various $\text{Li}_2[\text{Mn}_{1-2x}\text{Cr}_x\text{V}_x]\text{O}_3$ ($0 \leq x \leq 0.2$) samples after washing

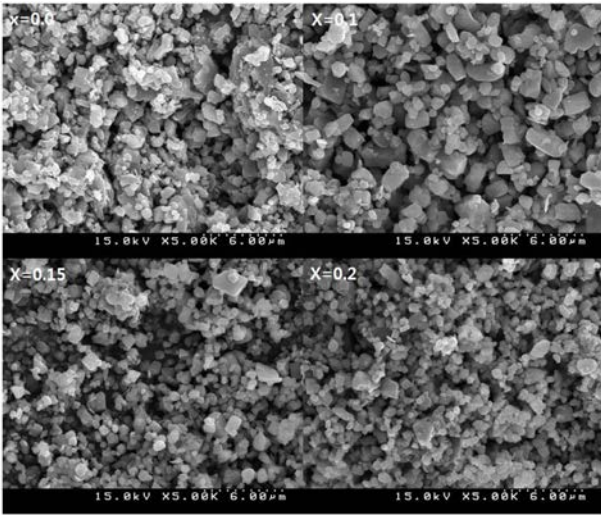


Fig. 3. S.E.M. images of $\text{Li}_2[\text{Mn}_{1-2x}\text{Cr}_x\text{V}_x]\text{O}_3$ ($0 \leq x \leq 0.2$) after washing.

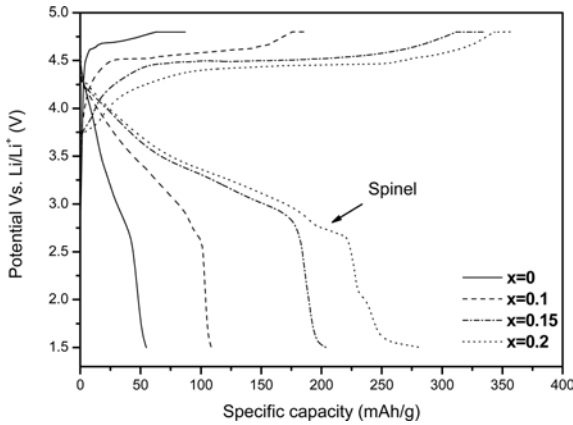


Fig. 4. The first charge/discharge profiles of various $\text{Li}_2[\text{Mn}_{1-2x}\text{Cr}_x\text{V}_x]\text{O}_3$ ($0 \leq x \leq 0.2$) samples after washing.

are shown in Fig. 4. The current of 10mA/g is applied between the potential range of 1.5–4.8 V vs. Li. All samples exhibit flat potential regions above 4.3 V in the first charge process. In the case of the first charge in Li_2MnO_3 , further oxidation of Mn^{4+} does not take place, and charging current is due to the delithiation compensated by the loss of oxygen [16]. The first charge capacities of $\text{Li}_{1.941}\text{MnO}_3$, $\text{Li}_{1.840}[\text{Mn}_{0.918}\text{Cr}_{0.077}\text{V}_{0.005}]\text{O}_3$, $\text{Li}_{1.781}[\text{Mn}_{0.873}\text{Cr}_{0.117}\text{V}_{0.010}]\text{O}_3$, and $\text{Li}_{1.596}[\text{Mn}_{0.806}\text{Cr}_{0.181}\text{V}_{0.013}]\text{O}_3$ are 87 mAh/g, 186 mAh/g, 334 mAh/g, and 359 mAh/g, respectively. As the doping content is increased, charge capacities are increased while average potentials are decreased. This result is similar with the previously reported composite cathode of $\text{Li}_2\text{MnO}_3 \cdot \text{LiMO}_2$ ($M = \text{Co}, \text{Ni}, \text{Cr}$) [12, 17, 18]. Different initial charging behaviors of Cr and V-doped sample depend on the relative amount of composite phases as well as the size of the particles. Although relatively a small amount of Li_2MnO_3 is expected in the sample of $\text{Li}_{1.781}[\text{Mn}_{0.873}\text{Cr}_{0.117}\text{V}_{0.010}]\text{O}_3$ and $\text{Li}_{1.596}[\text{Mn}_{0.806}\text{Cr}_{0.181}\text{V}_{0.013}]\text{O}_3$, the flat potential regions of charge process are extended. Electrochemical properties of the composite phases depend on the relative ratio of the each phase as well as the overall composition of the compounds.

For $\text{Li}_{1.596}[\text{Mn}_{0.806}\text{Cr}_{0.181}\text{V}_{0.013}]\text{O}_3$, an inflection region near 2.75 V in the discharge curve is observed. As shown in Fig. 2, this inflection behavior is related to the spinel $\text{Li}_{1+x}\text{Mn}_{2-x}\text{O}_4$ in the composite phase. Fig. 5 shows the results of cyclic voltammetry for the various $\text{Li}_2[\text{Mn}_{1-2x}\text{Cr}_x\text{V}_x]\text{O}_3$ ($0 \leq x \leq 0.2$) after washing. The results of 1st, 5th, and 10th cycles with the scan rate of 100 $\mu\text{V}/\text{s}$ in the potential range of 1.5–4.8 V vs. Li are reported. The oxidation peaks at ~ 4.6 V corresponding to the oxygen loss are observed in all samples. With the

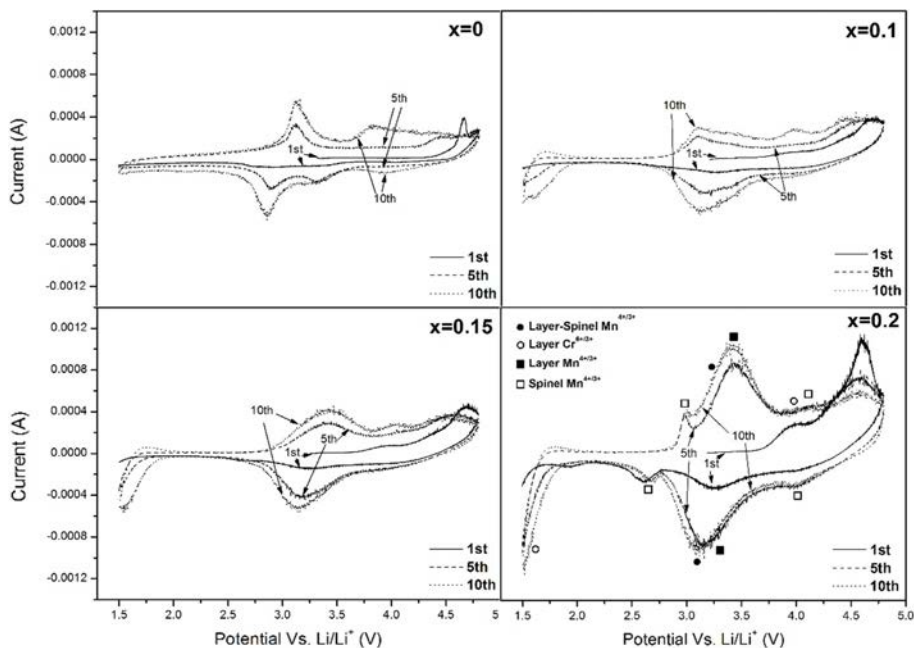


Fig. 5. Cyclic voltammograms for various $\text{Li}_2[\text{Mn}_{1-2x}\text{Cr}_x\text{V}_x]\text{O}_3$ ($0 \leq x \leq 0.2$) after washing.

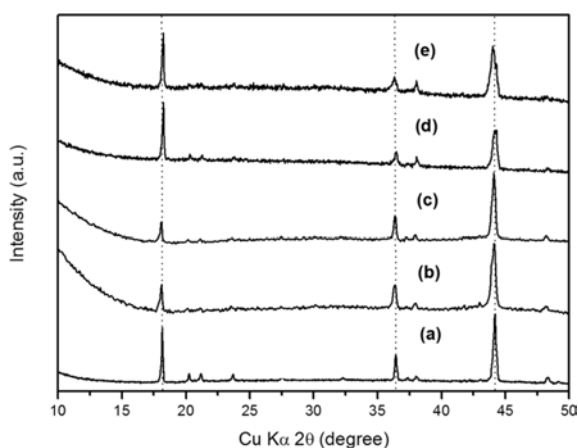


Fig. 6. Ex-situ XRD patterns of $\text{Li}_{1.781}[\text{Mn}_{0.873}\text{Cr}_{0.117}\text{V}_{0.010}]\text{O}_3$ electrodes for various potentials (a) OCV, (b) charged at 4.5 V, (c) charged at 4.8 V, (d) discharged at 2.7 V, (e) discharged at 1.5 V.

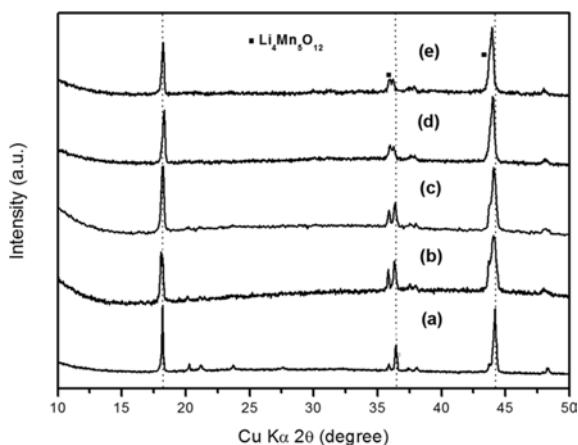


Fig. 7. Ex-situ XRD patterns of $\text{Li}_{1.596}[\text{Mn}_{0.806}\text{Cr}_{0.181}\text{V}_{0.013}]\text{O}_3$ electrodes for various potentials (a) OCV, (b) charged at 4.5 V, (c) charged at 4.8 V, (d) discharged at 2.7 V, (e) discharged at 1.5 V.

increase in Cr and V contents in the samples, an oxidation peak of Cr^{3+} to Cr^{6+} in $\text{LiCr}_{1-x}\text{V}_x\text{O}_2$ increases [18]. In the initial cycle of the sample with $x=0$, the reduction peaks appear at 3.3 and 2.8 V due to the reduction of Mn^{4+} to Mn^{3+} in layered LiMnO_2 and spinel LiMn_2O_4 , respectively. As Cr and V contents increase in the compounds, these two peaks merge into a single peak and exhibit a composite behavior. The reduction peaks moving to a lower potential with cycling indicate the phase transition from the layered phase to the spinel phase [13]. The reduction peak at 1.7 V due to the reduction of Cr^{6+} to Cr^{3+} increased level of Cr and V substitutions [18]. The sample of $x=0.2$ gives the oxidation at 3 V and reduction at 2.7 V, typical behaviors of the spinel phase.

In order to investigate structural changes of $\text{Li}_2[\text{Mn}_{1-2x}\text{Cr}_x\text{V}_x]\text{O}_3$ ($x=0.15$ and 0.2) during the charge and discharge process, ex-situ XRD measurements are carried out with the electrodes operated at various potentials. The results of XRD for $\text{Li}_{1.781}[\text{Mn}_{0.873}\text{Cr}_{0.117}\text{V}_{0.010}]\text{O}_3$ and $\text{Li}_{1.596}[\text{Mn}_{0.806}\text{Cr}_{0.181}\text{V}_{0.013}]\text{O}_3$ are shown in Fig. 6 and Fig. 7, respectively. As shown in Fig. 6(a) and Fig. 7(a), the electrodes at open circuit voltage have monoclinic layered structure (C2/m), and $\text{Li}_4\text{Mn}_5\text{O}_{12}$ phase is included in $\text{Li}_{1.596}[\text{Mn}_{0.806}\text{Cr}_{0.181}\text{V}_{0.013}]\text{O}_3$. The peaks between 20° and 35° decreased for the electrode charged at 4.5 V due to the delithiation in Li_2MnO_3 phase. (001) peak at $\sim 18.5^\circ$ in Fig. 6(b) is noticeably smaller than that in Fig. 7(b), and this indicates a structural change due to the larger oxygen loss during the initial charge for $\text{Li}_{1.781}[\text{Mn}_{0.873}\text{Cr}_{0.117}\text{V}_{0.010}]\text{O}_3$ compared to $\text{Li}_{1.596}[\text{Mn}_{0.806}\text{Cr}_{0.181}\text{V}_{0.013}]\text{O}_3$. Judging from the movement of major peaks, interplanar spacings increase with charge and decrease with discharge.

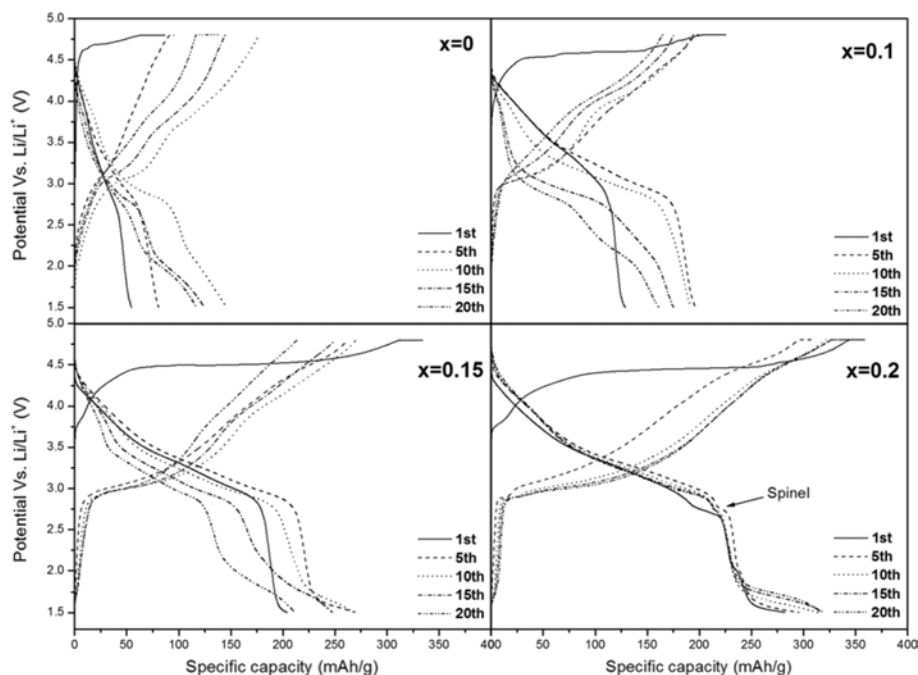


Fig. 8. Charge/discharge profiles of various $\text{Li}_2[\text{Mn}_{1-2x}\text{Cr}_x\text{V}_x]\text{O}_3$ ($0 \leq x \leq 0.2$) in the voltage range of 4.8-1.5 V vs. Li at 10 mA/g.

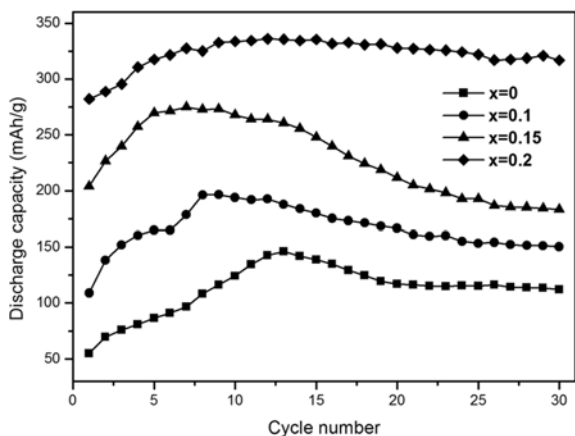


Fig. 9. Cyclabilities of the various $\text{Li}_2[\text{Mn}_{1-2x}\text{Cr}_x\text{V}_x]\text{O}_3$ ($0 \leq x \leq 0.2$) in the voltage range of 4.8-1.5 V vs. Li at 10 mA/g.

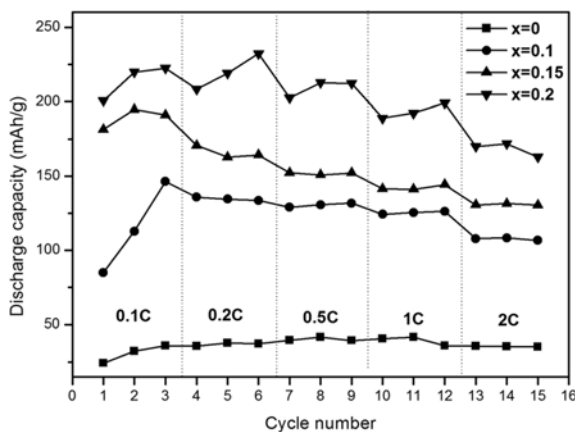


Fig. 10. Rate capabilities of various $\text{Li}_2[\text{Mn}_{1-2x}\text{Cr}_x\text{V}_x]\text{O}_3$ ($0 \leq x \leq 0.2$) in the voltage range of 4.8-1.5 V vs. Li at various C-rates.

Fig. 8 shows 1st, 5th, 10th, 15th, and 20th charge and discharge profiles of various $\text{Li}_2[\text{Mn}_{1-2x}\text{Cr}_x\text{V}_x]\text{O}_3$ ($0 \leq x \leq 0.2$) samples. Charge and discharge capacities depends on the amount of Cr and V substitution in the samples. For $\text{Li}_{1.596}[\text{Mn}_{0.806}\text{Cr}_{0.181}\text{V}_{0.013}]\text{O}_3$, the discharge capacity of 320 mAh/g is obtained for 20th cycle in the potential range of 4.8-1.5 V vs. Li. More importantly, Cr and V substituted Li_2MnO_3 can deliver more than 225 mAh/g of discharge capacity above 2.5 V vs. Li at 10 mA/g. In the case of $\text{Li}_2[\text{Mn}_{1-2x}\text{Cr}_x\text{V}_x]\text{O}_3$ ($0 \leq x \leq 1.5$), poor cycling behaviors are observed by the gradual phase transition from the layered phase to the spinel-like phase due to the repeated oxygen loss. As shown in Fig. 9 and Fig. 10, $\text{Li}_{1.596}[\text{Mn}_{0.806}\text{Cr}_{0.181}\text{V}_{0.013}]\text{O}_3$ has a composite phase of $\text{Li}_2\text{MnO}_3 \cdot \text{LiCrO}_2 \cdot \text{LiVO}_2 \cdot \text{Li}_4\text{Mn}_5\text{O}_{12}$ and exhibits a stable cycle performance as well as improved rate capabilities. Positive effects of Cr doping have been previously reported in the literature [18]. The substitution of Mn with Cr and V results in enhanced electrochemical behaviors of Li_2MnO_3 phase.

Conclusions

$\text{Li}_2[\text{Mn}_{1-2x}\text{Cr}_x\text{V}_x]\text{O}_3$ ($0 \leq x \leq 0.2$) are successfully

synthesized by an aqueous reduction reaction followed by heating in air. As-prepared sample include several impurities but these impurities can be removed by washing with DI water. XRD results suggest a structural change due to the lesser oxygen loss during the initial charge for $\text{Li}_{1.596}[\text{Mn}_{0.806}\text{Cr}_{0.181}\text{V}_{0.013}]\text{O}_3$ compared to other samples. Cr and V substituted Li_2MnO_3 can deliver more than 225 mAh/g of discharge capacity above 2.5 V vs. Li at 10 mA/g. Compared to other composition samples, $\text{Li}_{1.596}[\text{Mn}_{0.806}\text{Cr}_{0.181}\text{V}_{0.013}]\text{O}_3$ has a composite phase of $\text{Li}_2\text{MnO}_3 \cdot \text{LiCrO}_2 \cdot \text{LiVO}_2 \cdot \text{Li}_4\text{Mn}_5\text{O}_{12}$ and exhibits enhanced electrochemical performances.

Acknowledgments

This research was supported by the grants from the Fundamental R&D Program for Technology of World Premier Materials.

References

1. M.S. Whittingham, Chem. Rev. 104 (2004) 4271-4302.
2. P. Kalyani, S. Chitra, T. Mohan and S. Gopukumar, J. Power Sources 80 (1999) 103-106.
3. M.M. Thackeray, A. De Kock, M.H. Rossouw and D. Liles, J. Electrochem. Soc. 139 (1992) 363-366.
4. A. De Kock, M.H. Rossouw, L.A. de Picciotto and M.M. Thackeray, Mater. Res. Bull. 25 (1990) 657-664.
5. C.S. Johnson, J. Power Sources 165 (2007) 559-565.
6. S.H. Park, H.S. Ahn, G.J. Park, J. Kim and Y.S. Lee, Mater. Chem. Phys. 112 (2008) 696-701.
7. S.H. Park, Y. Sato, J.K. Kim and Y.S. Lee, Mater. Chem. Phys. 102 (2007) 225-230.
8. Y. Koyama, I. Tanaka, M. Nagao and R. Kanno, J. Power Sources 189 (2009) 798-801.
9. S.F. Amalraj, B. Markovsky, D. Sharon, M. Talianker, E. Zinigrad, R. Persky, O. Haik, J. Grinblat, J. Lampert, M.S. Dobrick, A. Garsuch, L. Burlaka and D. Aurbach, Electrochim. Acta 78 (2012) 32-39.
10. K.W. Kang, W.T. Kim and Y.U. Jeong, J. Ceram. Process Res. 14 (4) (2013) 468-471.
11. D.W. Yu and K. Yanagida, J. Electrochem. Soc. 158 (2011) A1015-A1022.
12. J.R. Croy, D.H. Kim, M. Balasubramanian, K. Gallagher, S.H. Kang and M.M. Thackeray, J. Electrochem. Soc. 159 (2012) A781-A790.
13. G. Singh, R. Thomas, A. Kumar and R.S. Katiyar, J. Electrochem. Soc. 159 (2012) A410-A420.
14. K. Numata, C. Sakaki and S. Yamanaka, Solid State Ionics 117 (1999) 257-263.
15. K. Nakamura, H. Hirano, Y. Michihiro and T. Moriga, Solid State Ionics 181 (2010) 1359-1365.
16. Z. Lu and J.R. Dahn, J. Electrochem. Soc. 149 (2002) A815-A822.
17. N. Yabuuchi, K. Yamamoto, K. Yoshii, I. Nakai, T. Nishizawa, A. Omaru, T. Toyooka, S. Komaba, J. Electrochem. Soc. 160 (2013) A39-A45.
18. Z. Lu and J.R. Dahn, J. Electrochem. Soc. 150 (2003) A1044-A1051.
19. A. Boulineau, L. Croguennec, C. Delmas, F. Weill, Solid State Ionics 180 (2010) 1652-1659.